



OPEN

Adsorption behavior and performance of ammonium onto sorghum straw biochar from water

Huajie Xu¹, Bing Wang^{2,3✉}, Ruohan Zhao², Xiangui Wang¹, Changbin Pan¹, Yuting Jiang¹, Xueyang Zhang⁴ & Banggui Ge⁵

Sorghum has been widely used for liquor production and brewing, but how to make efficiently utilize sorghum straw (SS) has become an urgent problem. Meanwhile, the wastewater produced by winemaking is typical organic wastewater with a high ammonium concentration. To solve the problem of resource utilization of SS and remove ammonium from water, SS was used to prepare biochar as an adsorbent for ammonium adsorption. Batch adsorption experiments were carried out to study the influencing factors and adsorption mechanisms of ammonium onto sorghum straw biochar (SSB). The results showed that the adsorption capacity of SSB was much higher than that of SS. The SSB pyrolyzed at 300 °C had the highest adsorption capacity. The favorable pH was 6–10, and the optimal dosage was 2.5 g/L. The adsorption process and behavior conformed to the pseudo-second-order kinetic and Langmuir isotherm adsorption models. The maximum ammonium adsorption capacity of SSB at 45 °C was 7.09 mg/g, which was equivalent to 7.60 times of SS. The ammonium adsorption of SS and SSB was mainly chemical adsorption. The regeneration test indicated that SSB had good regeneration performance after three adsorption-regeneration cycles. This work suggests that SSB could be potentially applied to sewage treatment containing ammonium to achieve the purpose of resource recycling.

Ammonium is one of the main forms of nitrogen in wastewater. A large amount of ammonium entering the water environment may result in serious environmental pollution and threaten human health^{1,2}. Therefore, effective control and removal of ammonium from wastewater to ensure the quality of the water environment are in need³. Nowadays, the commonly used treatments for removing ammonium in water mainly include ion exchange, chemical precipitation, adsorption, biological nitrification/denitrification, physical chemistry, etc.^{4–8}. Among them, the adsorption method is considered to be the most promising treatment method. It has the advantages of small equipment area, high removal efficiency, simple process, and renewable adsorbent⁹. However, there are many kinds of adsorbents with different adsorption effects^{10–12}. Although some adsorbents have good adsorption effects (such as activated carbon, clay minerals, carbon nanotubes, and graphene), the cost is higher than biochar prepared by straw waste. For example, the activation temperature of activated carbon is high, and the activation process is more complicated than biochar¹³. Therefore, the research and development of a low-cost and high-efficiency adsorbent have become a hot spot in this field.

As one of the main raw materials for liquor making, the planting area of sorghum has been increased with the increase of liquor production, resulting in a large amount of sorghum straw (SS) waste. In 2019, the yield of sorghum in China had reached 7.227 million tons. According to the ratio of sorghum to SS, it was estimated that the production of SS could reach 9.395 million tons¹⁴. Currently, SS resource utilization methods mainly include straw returning to the field, animal feed, straw energy, and straw substrate, etc. Due to the limitation of technical level, economy and market acceptance, the utilization rate of SS is still relatively low, with only a few parts of them are used as resources, and most of them are disposed of through open burning. It not only causes

¹Moutai Institute, Renhuai 564500, Guizhou, China. ²College of Resources and Environment Engineering, Guizhou University, Guiyang 550025, Guizhou, China. ³Key Laboratory of Karst Georesources and Environment, Ministry of Education, Guiyang 550025, Guizhou, China. ⁴School of Environmental Engineering, Xuzhou University of Technology, Xuzhou 221000, Jiangsu, China. ⁵Kweichow Moutai Co., Ltd, Renhuai 564500, Guizhou, China. ✉email: bwang6@gzu.edu.cn

a waste of resources but also results in pollution to the rural natural environment. Therefore, how to make full use of sorghum stalks as resources has become a challenge.

Biochar refers to a class of highly aromatic insoluble solid substances produced by pyrolysis (generally the carbonization temperature < 700 °C) and carbonization of organic materials such as crop straws, wood materials, and livestock manure under limited or without O₂ conditions^{15,16}. The well-developed porous structure and relatively large specific surface area (SSA) of biochar make it have good adsorption capacity¹⁷. Therefore, the application of biochar in environmental remediation has attracted much attention¹⁶. Biochar has been increasingly used as an adsorbent for pollutants such as heavy metals^{18–21}, chlorofluoro²², organic pollutants^{23,24}, phosphate^{25–28}, and ammonium, etc.^{2,28–32}. Cui et al. (2016) studied the adsorption effect of biochar prepared from six wetland biomass at 500 °C on ammonium and found that the canna biochar had the largest adsorption capacity (5.60 mg/g)²⁹. Huang et al. (2020) used clay/biochar composites to adsorb ammonium in water and found that the adsorption process was more in line with the pseudo-second-order kinetic model and Freundlich isotherm adsorption model³³. When Xue et al. (2019) used food waste-based biochar to adsorb ammonium in water, they found that the Langmuir equation was fit better to the adsorption behavior, and the adsorption of corn stalk biochar to ammonium was a spontaneous exothermic process. The maximum adsorption capacity was 7.174 mg/g³⁰. Wang et al. (2020c) used FeCl₃ and HCl to modify wheat straw biochar, and found that the ammonium adsorption capacity was improved by 14%³⁴. Although there have been many studies on the treatment of ammonium in wastewater using biochar from different feedstocks^{2,29,30,35}, few studies on the use of SS derived biochar to remove ammonium in water have been reported. The use of biochar prepared by SS can not only effectively adsorb pollutants, but also realize the resource utilization of straw waste. Therefore, the study of sorghum straw biochar (SSB) is in need.

As a kind of special biomass straw with extensive sources, SSB is supposed to be an adsorbent on ammonium in water. The main contents of this work are to (1) prepare and characterize SSB; (2) explore the influencing factors and adsorption mechanisms on ammonium in water with SSB, and (3) evaluate its adsorption and regeneration performance. This work could provide a theoretical basis for the potential application of SSB to absorb ammonium in wastewater and solve the resource utilization of SS.

Material and methods

Chemicals and materials. Main reagents: Nessler's reagent, ammonium chloride, potassium sodium tartrate, sulfuric acid, hydrochloric acid, sodium hydroxide, sodium carbonate, sodium bicarbonate, sodium ethoxide, etc. The above reagents are all analytical pure. Ultrapure water is used as test water. The ammonium stock solution is prepared with ammonium chloride to 1000 mg/L, and then diluted to the required ammonium concentration for different tests.

Main instruments: Scanning Electron Microscope (JSM-6610 LA, JEOL, Tokyo, Japan) (SEM). Fourier Transform Infrared Spectrometer (FTIR) (IRAffinity-1, Shimadzu, Japan). Pore Size and SSA Analyzer (Kubox1000, Beijing Builder Electronic Technology Co., Ltd). UV Spectrophotometer (UV-8000ST, Shanghai Yuanxi Instrument Co., Ltd). High-temperature tube furnace (SG-GL1200K, Shanghai Institute of Optics and Fine Mechanics).

Preparation and characterization of biochar. SS were collected from the organic sorghum base in the suburb of Renhuai City, Guizhou Province, which was obtained permission from the landowner (Supplementary materials). This experiment was carried out in accordance with the national standard from China entitled "Wood charcoal and test method of wood charcoal"³⁶. The preparation of SSB was following previous methods³⁷. After drying at 80 °C for 24 h, the SS was cut into 1 ~ 3 mm and then put into the tube furnace. At a heating rate of 2.5 °C/min, the carbonization temperature ranged from 300 to 600 °C under the condition of introducing N₂ and then kept at the target carbonization temperature for 30 min. After cooling, it was ground and passed through a 100–200 mesh sieve to obtain uniform biochar. Biochar prepared at temperatures of 300, 450, and 600 °C was labeled as SSB300, SSB450, SSB600.

Boehm titration method was used to determine the content of acidic oxygen-containing functional groups of biochar³⁸. Biochar morphology characteristics were scanned by SEM. The infrared spectrum of biochar was analyzed by FTIR. SSA, total pore volume, and average pore diameter of biochar were determined by BET-N₂.

Adsorption test. The concentration of ammonium was measured by Nessler's reagent method. Three parallel samples were adopted to control the quality of the analysis process. 50 mL PE centrifugal tubes were used to conduct all the adsorption experiments.

Adsorption influencing factors test. 0.1000 g of SSB300, SSB450, SSB600, and SS were weighed into test tubes. Then 40 mL ammonium solution (concentration of 50 mg/L, pH=7.0) was added and shaken at 25 °C for 1440 min. After shaking, the ammonium concentration of the supernatant was filtered and analyzed to obtain the biochar with optimal carbonization temperature for subsequent experiments. The optimal adsorbent experiment was selected in the range of 0.0250, 0.0500, 0.1000, 0.1250, 0.1500, 0.1750, and 0.2000 g. The effect of solution pH on the adsorption of ammonium was conducted by adjusting the solution pH from 2.0 to 12.0 by 0.1 mol/L NaOH and 0.1 mol/L HCl.

Adsorption kinetics and thermodynamic test. Sorption kinetics was examined at 25 °C with an interval time of 15, 30, 60, 120, 240, 480, 960, and 1440 min at the optimal adsorption conditions. Sorption isotherms were carried out by varying concentrations ranged from 0 to 250 mg/L at 25, 35, and 45 °C shaken for 24 h.

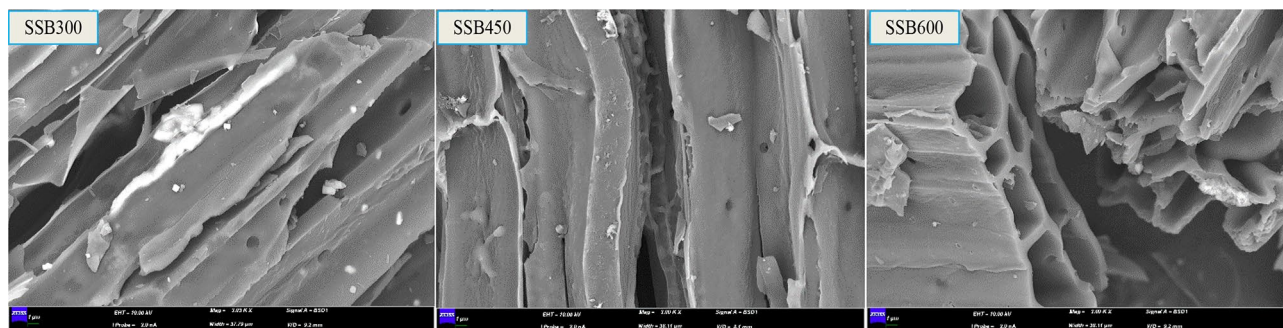


Figure 1. Scanning electron micrograph of biochar at different carbonization temperatures.

Biochars	Acidic oxygen-containing functional groups (mmol/g)				SSA (m ² /g)	Total pore volume (cm ³ /g)	Average pore size (nm)
	Carboxyl	Lactone group	Phenolic hydroxyl	Carbonyl			
SSB300	1.183	3.02	3.21	8.19	1.41	0.008	11.10
SSB450	0.716	1.99	2.27	5.86	43.51	0.036	1.67
SSB600	0.591	1.81	1.87	4.62	66.74	0.068	2.04

Table 1. The physicochemical properties of sorghum straw biochar.

Regeneration test. After reaching adsorption equilibrium, SS and SS300 were filtered out. Then 0.1 g SS and SS300 were put into 50 mL test tubes respectively and 40 mL of HCl and H₂SO₄ solutions were added (with a concentration of 0.1 mol/L)³⁹. After shaking for 1440 min at 25 °C, the samples were filtered and dried at 103 °C, and the above adsorption-regeneration tests were repeated several times.

Results and discussions

Physicochemical properties of biochar. The scanning electron microscope images of different biochar are shown in Fig. 1. The increasing carbonization temperature brings more obvious block layering and increases pore structure to biochar. The higher temperature leads to more organic matter decomposing in SS, which makes the biochar appear many micropores in the structure, resulting in the loose layering of the biochar⁴⁰. It shows that high carbonization temperature is beneficial to improve the SSA of biochar. From the physicochemical properties of SSB in Table 1, SSB300 has the highest average pore volume. Affected by the total pore volume, SSB600 has the highest SSA, and SSB300 has the lowest. The result coincides with the inference of the scanning electron microscope image.

From the analysis data in Table 1, SSB300 has the highest content of carboxyl, lactone, phenolic hydroxyl and carbonyl group, followed by SSB450 and SSB600. It is proved that the acidic functional groups can characterize hydrophilicity and ion exchange capacity gradually decrease with the increase of carbonization temperature⁴¹. Therefore, from the perspective of acidic oxygen-containing functional groups, SSB300 is more conducive to adsorption.

The infrared spectrum of SS and SSB are showed in Fig. 2. The absorption peak near 3417 cm⁻¹ is the -OH stretching vibration absorption peak⁴². The absorption peak gradually decreases with the increase of carbonization temperature. The increase of carbonization temperature improves the loss of hydroxyl during the pyrolysis process, thereby reducing the polarity of biochar. The absorption peaks near 2852 cm⁻¹ and 2919 cm⁻¹ are C-H symmetry and anti-symmetric stretching vibration absorption peaks of the methyl group in the alkyl group and the methylene group⁴³. The absorption peak gradually decreases with the increase of carbonization temperature, proving that carbonization temperature is proportional to the aromaticity of biochar. The absorption peaks near 1714 cm⁻¹ and 1100 cm⁻¹ are the C=O in the carboxyl group and the CO stretching vibration absorption peak in the ester group⁴⁴. As the carbonization temperature increases, these absorption peaks gradually decreases, proving that the polarity of biochar gradually decreases. The absorption peak near 1596 cm⁻¹ is the stretching vibration absorption peak of C=C on the aromatic ring and C=O in the carbonyl group⁴⁵. As the carbonization temperature increases, the peak gradually weakens. It may be that the carbonyl group in biochar is destroyed by high temperatures to generate CO and CO₂⁴⁶. The absorption peak near 875 cm⁻¹ is the C-H flexural vibration absorption peak on the aromatic ring⁴⁷. The absorption peak gradually increases with the increase of carbonization temperature, indicating that the stability and aromaticity of biochar are stronger. Therefore, from the analysis of infrared spectroscopy, the biochar contains a lot of oxygen-containing functional groups such as OH, COOH, and C=O, which gradually decreases as the carbonization temperature increases. The biochar pyrolyzes at low temperature is more conducive to adsorption, which is consistent with the results of oxygen-containing functional groups.

Adsorption influencing factors. *Carbonization temperature.* From Fig. 3, SSB300 had the highest adsorption capacity for ammonium, and the adsorption capacity and adsorption rate were 3.45 mg/g and 16.8%,

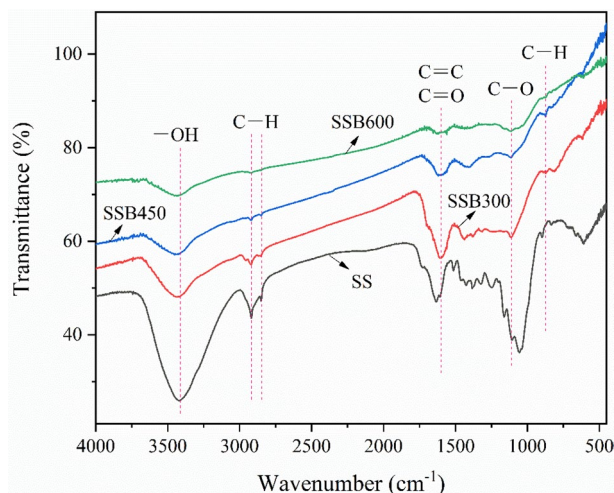


Figure 2. Infrared spectra of sorghum straw and its biochar.

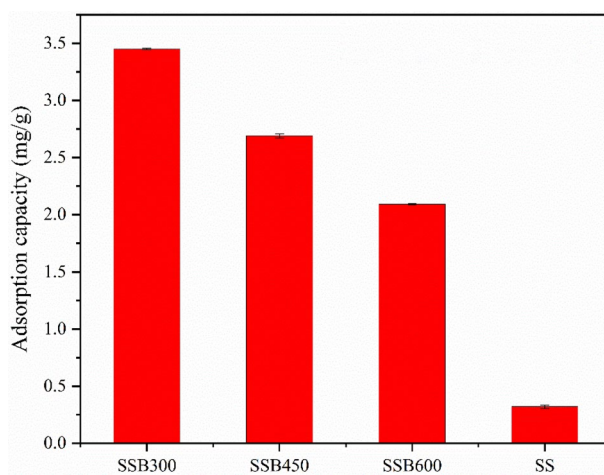


Figure 3. The adsorption capacity of biochar and sorghum straw for ammonium at different carbonization temperatures.

respectively. SS had the smallest adsorption capacity (0.321 mg/g). Overall, the adsorption capacity was in the order of SSB300 > SSB450 > SSB600 > SS. As carbonization temperature increased, the adsorption of ammonium by SSB had a downward trend. SS also had certain adsorption of ammonium, but its adsorption performance was much lower than SSB. Although SSB300 had the smallest SSA, it had the largest content of acidic oxygen-containing functional groups and stronger ion exchange capacity, which made the SSB300 had the largest adsorption of ammonium in water.

Adsorbent dosage. As shown in Fig. 4, with an increase of dosage, the adsorption capacity of SSB300 and SS for ammonium showed a downward trend, while the adsorption rates were upward. It was because as the amount of adsorbent increased, the SSA and adsorption pores of the adsorbent increased, thereby increasing the adsorption rate of ammonium. When the dosage of adsorbent was less than 0.1000 g, the ammonium adsorption rates of SSB300 and SS rose fast. When it exceeded 0.1000 g, the increasing trend was gentle, which indicated that more adsorbents can't effectively adsorb the ammonium in the water. Therefore, 0.1000 g was chosen as the optimal dosage for the test of SS and SSB to adsorb ammonium in water.

Solution pH. The adsorption effect of ammonium is greatly affected by pH⁴⁸. As shown in Fig. 5, when pH < 10, the ammonium adsorption capacity of SSB300 and SS rose with the increase of pH. Especially when the pH was 6–10, the adsorption capacity improved fast. When pH > 10, the adsorption of ammonium onto SSB300 and SS gradually decreased. The analysis believed that under acidic conditions, H⁺ facilitated the development

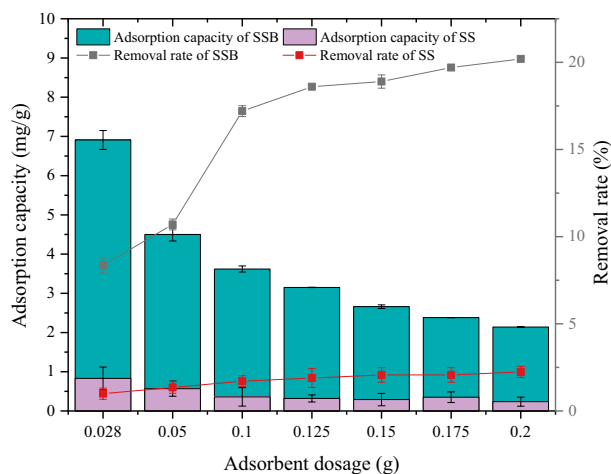


Figure 4. The effect of dosage on ammonium adsorption.

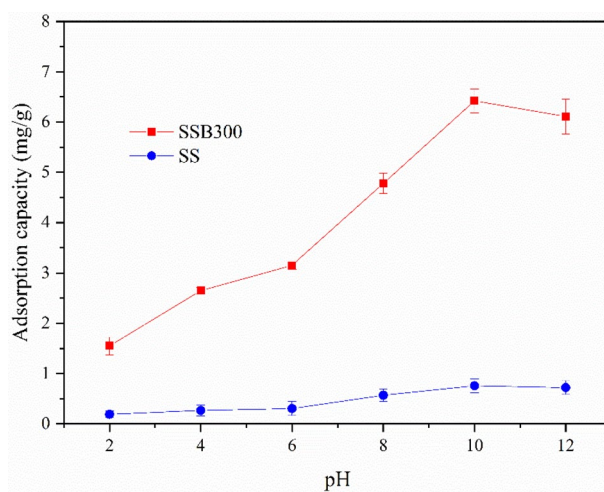


Figure 5. The effect of pH on ammonium adsorption.

of $\text{NH}_3\cdot\text{H}_2\text{O}$ ionization equilibrium toward NH_4^+ , thereby enhancing the adsorption of ammonium. But as the pH decreased, too much H^+ in the solution would bring competition to the adsorption of NH_4^+ , inhibiting the adsorption of ammonium³⁵. Under strong alkaline conditions ($\text{pH} > 10$), too much OH^- inhibited the ionization balance of $\text{NH}_3\cdot\text{H}_2\text{O}$, resulting in a decrease of NH_4^+ in the solution, thereby reducing the adsorption of ammonium. In addition, when $\text{pH} > 10$, a part of ammonium volatilized in gaseous form. Therefore, the optimal pH of SSB300 and SS for ammonium adsorption was in the range of neutral and slightly acidic to slightly alkaline (6 ~ 10). Considering the uniformity of the subsequent actual sewage treatment control test conditions, $\text{pH} = 7$ was selected for subsequent experiments.

Adsorption kinetics. The intraparticle diffusion model, the pseudo-first-order kinetic model and the pseudo-second-order kinetic model were used to fit the experimental data. The equations were shown in (1) ~ (3). The fitting curve was shown in Fig. 6, and the fitting parameters were shown in Table 2.

$$\text{Intraparticle diffusion model : } q_t = k_1 t^{1/2} + C \quad (1)$$

$$\text{Pseudo-first-order kinetic model: } q_t = q_e(1 - e^{-kt}) \quad (2)$$

$$\text{Pseudo-second-order kinetic model : } \frac{t}{q_t} = \frac{1}{k_3 q_e^2} + \frac{t}{q_e} \quad (3)$$

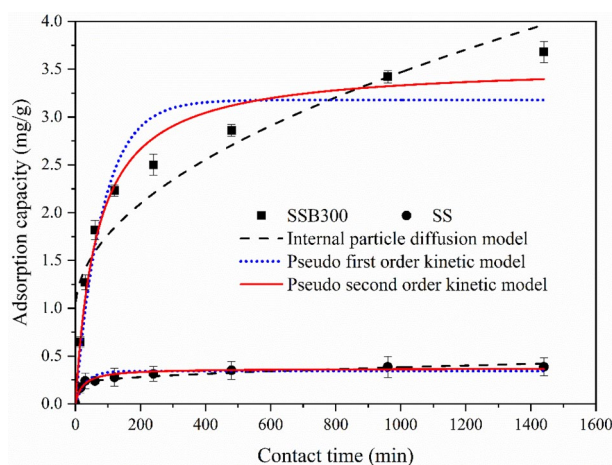


Figure 6. Ammonium adsorption kinetics fitting curve.

Adsorbents	Intraparticle diffusion model			Pseudo-first-order kinetic model			Pseudo-second-order kinetic model		
	C	k_1 ($\text{mg}\cdot\text{g}^{-1}\cdot\text{min}^{-0.5}$)	R^2	q_e ($\text{mg}\cdot\text{g}^{-1}$)	K_2 min^{-1}	R^2	q_e ($\text{mg}\cdot\text{g}^{-1}$)	K_3 ($\text{mg}\cdot\text{g}^{-1}\cdot\text{min}^{-1}$)	R^2
SSB300	0.9830	0.0786	0.8718	3.1786	0.0121	0.9218	3.5529	0.0042	0.9733
SS	0.1960	0.0059	0.8490	0.3416	0.0329	0.8758	0.3694	0.1208	0.9526

Table 2. Fitting parameters of ammonium adsorption kinetics.

where q_t represents the adsorption capacity of ammonium at time t , mg/g . q_e is the adsorption capacity of ammonium at adsorption equilibrium, mg/g . k_1 , k_2 , k_3 are adsorption rate constants; C is a constant.

As shown in Table 2 and Fig. 6, the correlation coefficient R^2 of the pseudo-second-order kinetic model was the highest, and the R^2 of SSB300 was higher than that of SS. The theoretical equilibrium adsorption capacities were 3.55 and 0.375 mg/g respectively, which were very close to the actual saturated adsorption capacities (3.68 and 0.388 mg/g). Therefore, the pseudo-second-order kinetic model was more consistent with the adsorption process of SS and SSB300 on ammonium in water.

From the perspective of the particle diffusion model, the adsorption process of SS and SSB300 on ammonium in water could be roughly divided into two stages. The first 3 h was the process of rapid adsorption of ammonium onto the surface of the adsorbent. Phase 2: After 3 h ammonium diffused slowly into the adsorbent. Due to the influence of molecular diffusion resistance, the diffusion rate within the adsorption decreased until the adsorption tended to balance. This stage was the rate-controlling stage of ammonium adsorption. Due to $C \neq 0$, it indicated that intra-particle diffusion was not the only speed control step, meaning that the fitting curve was not at the origin⁴⁹. The adsorption rate might be controlled by surface adsorption and intra-particle diffusion^{50,51}.

Adsorption isotherms. The Freundlich and Langmuir isotherm adsorption models were fitted to the adsorption test data at 25, 35, and 45 °C. The fitting curves were shown in Figs. 7 and 8, respectively, and the fitting parameters were shown in Table 3. The equations of the Freundlich and Langmuir isotherm adsorption models were as follows:

$$\text{Freundlich model : } q_e = k_F C_e^{1/n} \quad (4)$$

$$\text{Langmuir model : } q_e = \frac{q_m k_L C_e}{1 + k_L C_e} \quad (5)$$

In the above formula, q_m is the theoretical maximum adsorption capacity of ammonium, mg/g . C_e is the concentration of ammonium in the solution at adsorption equilibrium, mg/L . k_B , k_L , n are isotherm constants.

As shown in Table 3, Figs. 7 and 8, the correlation coefficient R^2 of the Langmuir isotherm adsorption model was higher than that of the Freundlich isotherm adsorption model, proving that the Langmuir isotherm adsorption model was more in line with the thermodynamic adsorption behavior of SS and SSB300 for ammonium in water. And they were mainly monolayer adsorption. At 25, 35, and 45 °C, the maximum adsorption capacity of SSB300 for ammonium was 6.77, 6.97, and 7.09 mg/g , respectively, which was equivalent to 8.65, 8.64, and 7.60 times of SS. Compared with other adsorbents, SSB300 in this study showed a high ammonium adsorption capacity (Table 4). This difference was mainly attributed to the differences in physical and chemical properties between different biochar.

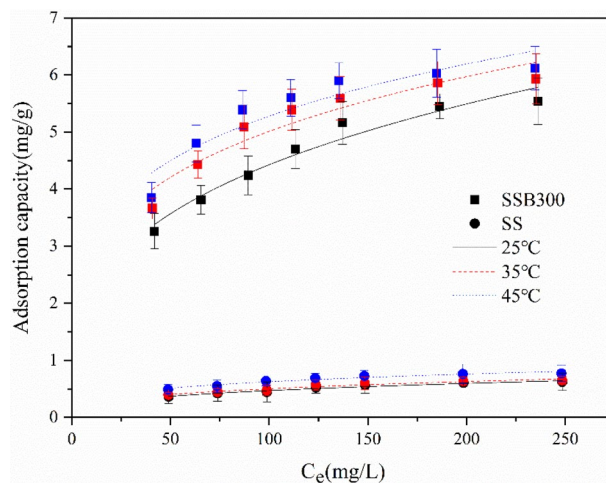


Figure 7. The adsorption thermodynamic isotherm of ammonium (Freundlich).

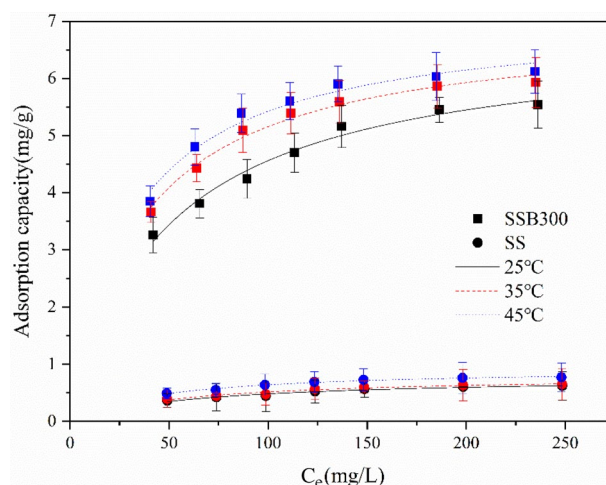


Figure 8. The adsorption thermodynamic isotherm of ammonium (Langmuir).

Adsorbents	T(K)	Freundlich model			Langmuir model			
		K_f (L/mg)	$1/n$	R^2	q_m (mg/g)	K_L (L/mg)	R^2	R_L
SSB300	298	1.0553	0.3113	0.9541	6.7655	0.0207	0.9779	0.162~0.491
	308	1.5630	0.2530	0.8979	6.9687	0.0284	0.9838	0.123~0.423
	318	1.8252	0.2306	0.8599	7.0930	0.0325	0.9699	0.110~0.381
SS	298	0.0968	0.3431	0.9539	0.7817	0.0161	0.9608	0.199~0.544
	308	0.1135	0.3234	0.9339	0.8068	0.0177	0.9458	0.184~0.531
	318	0.1703	0.2824	0.9295	0.9336	0.0218	0.9785	0.155~0.478

Table 3. Isothermal adsorption fitting parameters of ammonium.

In addition, the separation factor R_L was used to judge the adsorption effectiveness of the adsorbent⁵⁶. The equation was:

$$\text{Separation factor : } R_L = \frac{1}{1 + k_L C_0} \tag{6}$$

C_0 —The initial concentration of ammonium in the solution, mg/L.

Among them, $R_L = 0$ is irreversible adsorption. $0 < R_L < 1$ is favorable adsorption. $R_L = 1$ is linear adsorption.

Biochars	Adsorption capacity (mg/g)	References
Wood chips biochar	0.96	52
Sludge biochar	1.2	53
Bamboo biochar	7.0	54
Coffee husk biochar	2.8	55
Canna biochar	5.6	29
Corn stalk biochar	7.174	30
Sorghum straw biochar	7.09	This study

Table 4. A comparison of the adsorption capacities of other adsorbents for ammonium.

Adsorbents	T(K)	Langmuir model		ΔG^θ (kJ/mol)	ΔH^θ (kJ/mol)	ΔS^θ (kJ/mol-K)
		K_L (L/mg)	K_L^θ			
SSB300	298	0.0207	3067.8 ^a	-19.89	-24.03	-0.1417
	308	0.0284	2025.4 ^a	-18.86		
	318	0.0325	1670.4 ^a	-18.39		
SS	298	0.0161	2.98×10^{5a}	-31.23	-26.76	0.1553
	308	0.0177	2.54×10^{5a}	-30.83		
	318	0.0218	1.50×10^{5a}	-29.54		

Table 5. The adsorption thermodynamic parameters of ammonium. ^aWhen calculating the molar concentration of the adsorbent, the molecular weights of SSB300 and SS were assumed to be the molecular weight of C (12 g/mol).

From Table 3, the R_L of SS and SSB300 at the three temperatures was all greater than 0 but less than 1, indicating that the SS and SSB had favorable adsorption of ammonium in water.

Adsorption thermodynamics. Judging from the isotherm adsorption models of SS and SSB300 at 3 temperatures, the adsorption capacity gradually increased as the temperature improved. To further study the thermodynamic behavior of adsorption, the Gibbs free energy change, enthalpy change and entropy change were analyzed according to the Langmuir isotherm adsorption model parameters in Table 3. The calculation formula was as follows:

$$\Delta G^\theta = -RT \ln K_L^\theta = \Delta H^\theta - TS^\theta \quad (7)$$

$$\ln K_L^\theta = \frac{\Delta S^\theta}{R} - \frac{\Delta H^\theta}{RT} \quad (8)$$

In the above formula, ΔG^θ is Gibbs free energy change, kJ/mol. ΔH^θ is enthalpy change, kJ/mol. ΔS^θ is entropy change, kJ/mol. R is gas constant, J/mol-K. K_L^θ is the standard equilibrium constant, that is, the Langmuir isotherm adsorption model empirical equilibrium constant after standard concentration correction, dimensionless.

The Gibbs free energy change, enthalpy change and entropy change calculated by formulas (7) and (8) are shown in Table 5.

From the results in Table 5, $\Delta G^\theta < 0$, showed that the adsorption process of SS and SSB to ammonium in water was spontaneous. The ΔH^θ of SS and SSB300 were both less than 0, indicating that the adsorption process of SS and SSB to ammonium in water was exothermic.

Adsorption mechanisms. According to the results of BET, FTIR and SEM analysis of SSB, the biochar with higher carbonization temperature had higher SSA and pore volume. However, adsorption results showed that biochar with low carbonization temperature had the best adsorption effect on ammonium in water. Through the analysis of the oxygen-containing functional group test results and the FTIR diagram of the biochar, it was found that the biochar with lower carbonization temperature contained more oxygen-containing functional groups, which was more conducive to the adsorption of ammonium. This analysis result was consistent with the actual adsorption results. It proved that the adsorption of SSB to ammonium in water was not simply physical adsorption, but a complex physical and chemical adsorption process dominated by chemical adsorption⁵¹. From the perspective of adsorption kinetics, the adsorption process was more in line with pseudo-second-order kinetics, which was consistent with the mechanism of clay/biochar composite adsorption particles on ammonium³³. From the perspective of isothermal adsorption, the Langmuir isotherm adsorption model was more consistent with the adsorption behavior of SS and SSB on ammonium in water, which was consistent with the adsorption

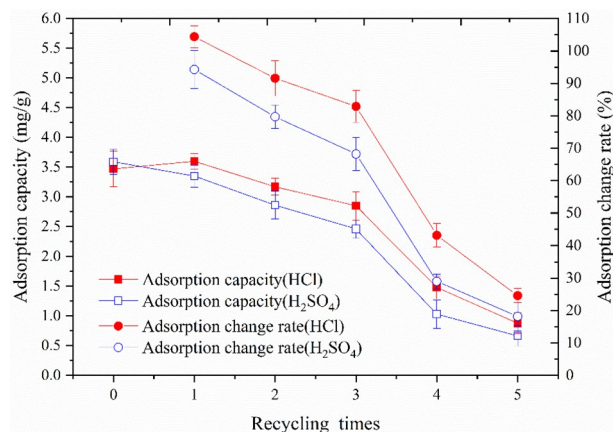


Figure 9. Adsorption effect under different regeneration conditions.

mechanism of food waste-based biochar on ammonium in water³⁰. The thermodynamic analysis proved that the adsorption process was mainly chemical adsorption, which was a spontaneous and exothermic process.

Regeneration performance. To investigate the regeneration performance of SS and SS300 after adsorbing ammonium, they were regenerated with HCl and H₂SO₄ solutions respectively. The adsorption effect after regeneration was shown in Fig. 9. The adsorption capacity of SS and SS300 after regeneration by HCl solution was higher than that of H₂SO₄ solution. With repeated experiments of adsorption-regeneration, the first 3 adsorption-regeneration cycles of SS300 changed slightly. It was determined that the optimal number of regenerations of SS300 under the condition of HCl solution was 3, and the equilibrium adsorption capacity after regeneration was 82.1% of the initial adsorption capacity. Since the adsorption capacity of SS was very small, the adsorption capacity became extremely low after the first adsorption-regeneration cycle. Therefore, the regeneration performance of SS after adsorbing ammonium was extremely low, while the SSB had good regeneration performance after adsorbing ammonium.

Conclusions

SS and SSB can adsorb ammonium well in water. The adsorption of ammonium onto SSB is much higher than that of SS. The favorable pH for ammonium adsorption is 6–10 and the optimal dosage is 2.5 g/L. Low carbonization temperature (300 °C) is more conducive to the formation of functional groups, which are beneficial to the adsorption of ammonium. The adsorption process of SS and SSB to ammonium in water is more in line with the pseudo-second-order kinetic model. The adsorption behavior is more in line with the Langmuir isotherm adsorption model. The maximum ammonium adsorption capacity at 25, 35, and 45 °C are 6.77, 6.97, and 7.09 mg/g, which are equivalent to 8.65, 8.64, and 7.60 times of SS, respectively. And the adsorption process is spontaneous and exothermic. The study indicates that SSB can be applied to sewage treatment containing ammonium to achieve the purpose of resource recycling.

Received: 27 July 2021; Accepted: 9 March 2022

Published online: 30 March 2022

References

- Ke, X., Bao, Q. H., Qi, Y. F., Huang, X. Y. & Zhang, H. J. Toxicity assessment of sediments from the Liaohe River Protected Area (China) under the influence of ammonia nitrogen, heavy metals and organic contaminants. *Environ. Toxicol. Pharmacol.* **59**, 34–42. <https://doi.org/10.1016/j.etap.2018.02.008> (2018).
- Yao, F. *et al.* Preparation and characterization of a copper phosphotungstate/titanium dioxide (Cu-H₃PW₁₂O₄₀/TiO₂) composite and the photocatalytic oxidation of high-concentration ammonia nitrogen. *Sci. Total Environ.* **727**, 138425. <https://doi.org/10.1016/j.scitotenv.2020.138425> (2020).
- Van Kessel, M. A. *et al.* Current perspectives on the application of N-damo and anammox in wastewater treatment. *Curr. Opin. Biotechnol.* **50**, 222–227. <https://doi.org/10.1016/j.copbio.2018.01.031> (2018).
- Nancharaiyah, Y. V., Venkata Mohan, S. & Lens, P. N. L. Recent advances in nutrient removal and recovery in biological and bioelectrochemical systems. *Bioresour. Technol.* **215**, 173–185. <https://doi.org/10.1016/j.biortech.2016.03.129> (2016).
- Feng, C. *et al.* Synchronous removal of ammonium and phosphate from swine wastewater by two agricultural waste based adsorbents: Performance and mechanisms. *Biores. Technol.* **307**, 123231. <https://doi.org/10.1016/j.biortech.2020.123231> (2020).
- An, Y. *et al.* Decreasing ammonium generation using hydrogenotrophic bacteria in the process of nitrate reduction by nanoscale zero-valent iron. *Sci. Total Environ.* **407**, 5465–5470. <https://doi.org/10.1016/j.scitotenv.2009.06.046> (2009).
- Huang, H., Xiao, X., Yan, B. & Yang, L. Ammonium removal from aqueous solutions by using natural Chinese (Chende) zeolite as adsorbent. *J. Hazard. Mater.* **175**, 247–252. <https://doi.org/10.1016/j.jhazmat.2009.09.156> (2010).
- Yan, A., Liu, C., Liu, Y. & Xu, F. Effect of ion exchange on the rate of aerobic microbial oxidation of ammonium in hyporheic zone sediments. *Environ. Sci. Pollut. Res.* **25**, 8880–8887. <https://doi.org/10.1007/s11356-018-1217-x> (2018).

9. Zhao, Y. X. *et al.* Adsorption of high ammonium nitrogen from wastewater using a novel ceramic adsorbent and the evaluation of the ammonium-adsorbed-ceramic as fertilizer. *J. Colloid Interface Sci.* **393**, 264–270. <https://doi.org/10.1016/j.jcis.2012.10.028> (2013).
10. Su, J., Huang, H. G., Jin, X. Y., Lu, X. Q. & Chen, Z. L. Synthesis, characterization and kinetic of a surfactant-modified bentonite used to remove As(III) and As(V) from aqueous solution. *J. Hazard. Mater.* **185**, 63–70. <https://doi.org/10.1016/j.jhazmat.2010.08.122> (2011).
11. Ahmad, M. *et al.* Biochar as a sorbent for contaminant management in soil and water: A review. *Chemosphere* **99**, 19–33. <https://doi.org/10.1016/j.chemosphere.2013.10.071> (2014).
12. Sun, Z., Qu, X., Wang, G., Zheng, S. & Frost, R. L. Removal characteristics of ammonium nitrogen from wastewater by modified Ca-bentonites. *Appl. Clay Sci.* **107**, 46–51. <https://doi.org/10.1016/j.clay.2015.02.003> (2015).
13. Danish, M. & Ahmad, T. A review on utilization of wood biomass as a sustainable precursor for activated carbon production and application. *Renew. Sustain. Energy Rev.* **87**, 1–21. <https://doi.org/10.1016/j.rser.2018.02.003> (2018).
14. Li, S. *et al.* Current status and future prospective of sorghum production and seed industry in China. *Sci. Agric. Sin.* **54**(3), 471–482. <https://doi.org/10.3864/j.issn.0578-1752.2021.03.002> (2021).
15. Lehmann, J. & Joseph, S. *Biochar for Environmental Management: Science, Technology and Implementation* (Routledge, 2015).
16. Wang, B., Gao, B. & Fang, J. Recent advances in engineered biochar productions and applications. *Crit. Rev. Environ. Sci. Technol.* **47**, 2158–2207. <https://doi.org/10.1080/10643389.2017.1418580> (2018).
17. Joseph, S. D. *et al.* An investigation into the reactions of biochar in soil. *Aust. J. Soil Res.* **48**, 501–515. <https://doi.org/10.1071/Sr10009> (2010).
18. Liu, L., Liu, X., Wang, D., Lin, H. & Huang, L. Removal and reduction of Cr(VI) in simulated wastewater using magnetic biochar prepared by co-pyrolysis of nano-zero-valent iron and sewage sludge. *J. Clean. Prod.* **257**, 120562. <https://doi.org/10.1016/j.jclepro.2020.120562> (2020).
19. Lian, G. *et al.* Enhanced removal of hexavalent chromium by engineered biochar composite fabricated from phosphogypsum and distillers grains. *Sci. Total Environ.* **697**, 134119. <https://doi.org/10.1016/j.scitotenv.2019.134119> (2019).
20. Kwon, G., Bhatnagar, A., Wang, H., Kwon, E. E. & Song, H. A review of recent advancements in utilization of biomass and industrial wastes into engineered biochar. *J. Hazard. Mater.* **400**, 123242. <https://doi.org/10.1016/j.jhazmat.2020.123242> (2020).
21. Zhao, R. *et al.* Fabrication and environmental applications of metal-containing solid waste/biochar composites: A review. *Sci. Total Environ.* <https://doi.org/10.1016/j.scitotenv.2021.149295> (2021).
22. Mei, L. P. *et al.* One-step synthesis of zirconium dioxide-biochar derived from *Camellia oleifera* seed shell with enhanced removal capacity for fluoride from water. *Appl. Surf. Sci.* **509**, 144685. <https://doi.org/10.1016/j.apsusc.2019.144685> (2020).
23. Lonappan, L. *et al.* Adsorption of methylene blue on biochar microparticles derived from different waste materials. *Waste Manage.* **49**, 537–544. <https://doi.org/10.1016/j.wasman.2016.01.015> (2016).
24. Gan, Q. *et al.* Sludge-derived biochar with multivalent iron as an efficient Fenton catalyst for degradation of 4-Chlorophenol. *Sci. Total Environ.* **725**, 138299. <https://doi.org/10.1016/j.scitotenv.2020.138299> (2020).
25. Wang, B. *et al.* Phosphogypsum as a novel modifier for distillers grains biochar removal of phosphate from water. *Chemosphere* **238**, 124684. <https://doi.org/10.1016/j.chemosphere.2019.124684> (2020).
26. Cho, D.-W. *et al.* Fabrication and environmental applications of multifunctional mixed metal-biochar composites (MMBC) from red mud and lignin wastes. *J. Hazard. Mater.* **374**, 412–419. <https://doi.org/10.1016/j.jhazmat.2019.04.071> (2019).
27. Qiu, B. & Duan, F. Synthesis of industrial solid wastes/biochar composites and their use for adsorption of phosphate: From surface properties to sorption mechanism. *Colloids Surf., A* **571**, 86–93. <https://doi.org/10.1016/j.colsurfa.2019.03.041> (2019).
28. Dai, Y., Wang, W., Lu, L., Yan, L. & Yu, D. Utilization of biochar for the removal of nitrogen and phosphorus. *J. Clean. Prod.* **257**, 120573. <https://doi.org/10.1016/j.jclepro.2020.120573> (2020).
29. Cui, X. Q., Hao, H. L., Zhang, C. K., He, Z. L. & Yang, X. E. Capacity and mechanisms of ammonium and cadmium sorption on different wetland-plant derived biochars. *Sci. Total Environ.* **539**, 566–575. <https://doi.org/10.1016/j.scitotenv.2015.09.022> (2016).
30. Xue, S. *et al.* Food waste based biochars for ammonia nitrogen removal from aqueous solutions. *Bioresour. Technol.* <https://doi.org/10.1016/j.biortech.2019.121927> (2019).
31. Wang, B., Lehmann, J., Hanley, K., Hestrin, R. & Enders, A. Adsorption and desorption of ammonium by maple wood biochar as a function of oxidation and pH. *Chemosphere* **138**, 120–126. <https://doi.org/10.1016/j.chemosphere.2015.05.062> (2015).
32. Wang, B., Lehmann, J., Hanley, K., Hestrin, R. & Enders, A. Ammonium retention by oxidized biochars produced at different pyrolysis temperatures and residence times. *RSC Adv.* **6**, 41907–41913. <https://doi.org/10.1039/c6ra06419a> (2016).
33. Huang, X. *et al.* Preparation of clay/biochar composite adsorption particle and performance for ammonia nitrogen removal from aqueous solution. *J. Ocean Univers. China* **19**, 729–739. <https://doi.org/10.1007/s11802-020-4150-9> (2020).
34. Wang, S. *et al.* Carboxyl and hydroxyl groups enhance ammonium adsorption capacity of iron (III) chloride and hydrochloric acid modified biochars. *Biores. Technol.* **309**, 123390. <https://doi.org/10.1016/j.biortech.2020.123390> (2020).
35. Zhang, M. *et al.* Evaluating biochar and its modifications for the removal of ammonium, nitrate, and phosphate in water. *Water Res.* **186**, 116303. <https://doi.org/10.1016/j.watres.2020.116303> (2020).
36. Supervision, N. B. o. Q. a. T. Vol. GB/T 17664–1999, (China Standard Press, 1999).
37. Wang, B. *et al.* Environmental-friendly coal gangue-biochar composites reclaiming phosphate from water as a slow-release fertilizer. *Sci. Total Environ.* <https://doi.org/10.1016/j.scitotenv.2020.143664> (2020).
38. Vithanage, M. *et al.* Mechanisms of antimony adsorption onto soybean stover-derived biochar in aqueous solutions. *J. Environ. Manage.* **151**, 443–449. <https://doi.org/10.1016/j.jenvman.2014.11.005> (2015).
39. Dai, Y., Zhang, N., Xing, C., Cui, Q. & Sun, Q. The adsorption, regeneration and engineering applications of biochar for removal organic pollutants: A review. *Chemosphere* **223**, 12–27. <https://doi.org/10.1016/j.chemosphere.2019.01.161> (2019).
40. Leng, L. & Huang, H. An overview of the effect of pyrolysis process parameters on biochar stability. *Biores. Technol.* **270**, 627–642. <https://doi.org/10.1016/j.biortech.2018.09.030> (2018).
41. Wahab, M. A., Boubakri, H., Jellali, S. & Jedidi, N. Characterization of ammonium retention processes onto Cactus leaves fibers using FTIR, EDX and SEM analysis. *J. Hazard. Mater.* **241**, 101–109. <https://doi.org/10.1016/j.jhazmat.2012.09.018> (2012).
42. N, V. V., M, Z., S, K, B. & H.-S., P., Arsenic(III) removal from aqueous solution by raw and zinloaded pine cone biochar: equilibrium, kinetics, and thermodynamics studies. *Environ. Sci. Technol.* **12**(4), 1283–1294. <https://doi.org/10.1007/s13762-014-0507-1> (2014).
43. Zheng, H. *et al.* Characteristics and nutrient values of biochars produced from giant reed at different temperatures. *Biores. Technol.* **130**, 463–471. <https://doi.org/10.1016/j.biortech.2012.12.044> (2013).
44. Reichberger, M. V. *et al.* Changes in biochar physical and chemical properties: Accelerated biochar aging in an acidic soil. *Carbon* **115**, 209–219. <https://doi.org/10.1016/j.carbon.2016.12.096> (2017).
45. Inyang, M., Gao, B., Zimmerman, A., Zhou, Y. M. & Cao, X. D. Sorption and cosorption of lead and sulfapyridine on carbon nanotube-modified biochars. *Environ. Sci. Pollut. Res.* **22**, 1868–1876. <https://doi.org/10.1007/s11356-014-2740-z> (2015).
46. Zhang, X. Y. *et al.* Biochar for volatile organic compound (VOC) removal: Sorption performance and governing mechanisms. *Biores. Technol.* **245**, 606–614. <https://doi.org/10.1016/j.biortech.2017.09.025> (2017).
47. Tan, X. F. *et al.* Application of biochar for the removal of pollutants from aqueous solutions. *Chemosphere* **125**, 70–85. <https://doi.org/10.1016/j.chemosphere.2014.12.058> (2015).

48. Vu, T. M. *et al.* Removing ammonium from water using modified corncob-biochar. *Sci. Total Environ.* **579**, 612–619. <https://doi.org/10.1016/j.scitotenv.2016.11.050> (2017).
49. Arami, M., Limaee, N. Y. & Mahmoodi, N. M. Evaluation of the adsorption kinetics and equilibrium for the potential removal of acid dyes using a biosorbent. *Chem. Eng. J.* **139**, 2–10. <https://doi.org/10.1016/j.cej.2007.07.060> (2008).
50. Vadivelan, V. & Kumar, K. V. Equilibrium, kinetics, mechanism, and process design for the sorption of methylene blue onto rice husk. *J. Colloid Interface Sci.* **286**, 90–100. <https://doi.org/10.1016/j.jcis.2005.01.007> (2005).
51. Fan, R. *et al.* Adsorption characteristics of ammonium ion onto hydrous biochars in dilute aqueous solutions. *Biores. Technol.* **272**, 465–472. <https://doi.org/10.1016/j.biortech.2018.10.064> (2019).
52. Begum, S. A., Golam Hyder, A. H. M., Hicklen, Q., Crocker, T. & Oni, B. Adsorption characteristics of ammonium onto biochar from an aqueous solution. *J. Water Supply Res. Technol. Aqua* **70**, 113–122. <https://doi.org/10.2166/aqua.2020.062> (2021).
53. Tang, Y. *et al.* Influence of pyrolysis temperature on production of digested sludge biochar and its application for ammonium removal from municipal wastewater. *J. Clean. Prod.* **209**, 927–936. <https://doi.org/10.1016/j.jclepro.2018.10.268> (2019).
54. Qin, Y. *et al.* Enhanced removal of ammonium from water by ball-milled biochar. *Environ. Geochem. Health* **42**, 1579–1587. <https://doi.org/10.1007/s10653-019-00474-5> (2020).
55. Vu, N.-T. & Do, K.-U. Insights into adsorption of ammonium by biochar derived from low temperature pyrolysis of coffee husk. *Biomass Convers. Biorefin.* <https://doi.org/10.1007/s13399-13021-01337-13399> (2021).
56. Zhao, Y. F. *et al.* Preparation of highly ordered cubic NaA zeolite from halloysite mineral for adsorption of ammonium ions. *J. Hazard. Mater.* **178**, 658–664. <https://doi.org/10.1016/j.jhazmat.2010.01.136> (2010).

Acknowledgements

This work was supported by the National Natural Science Foundation of China (41977297), the Special Research Fund of Natural Science (Special Post) of Guizhou University [(2020)01], the Key Cultivation Program of Guizhou University [2019(08)] and the Youth Science and Technology Talent Project of the Education Department in Guizhou Province [(2018)464].

Author contributions

H.X.: Experiments, writing, and data processing. B.W.: Guidance, supervision, review, editing, and revision. R.Z.: Writing, review, and editing. X.W.: Experimental assistance. C.P.: Experimental assistance. Y.J.: Experimental assistance. X.Z.: Samples analysis and characterization. B.G.: Experimental assistance.

Competing interests

The authors declare no competing interests.

Additional information

Supplementary Information The online version contains supplementary material available at <https://doi.org/10.1038/s41598-022-08591-5>.

Correspondence and requests for materials should be addressed to B.W.

Reprints and permissions information is available at www.nature.com/reprints.

Publisher's note Springer Nature remains neutral with regard to jurisdictional claims in published maps and institutional affiliations.



Open Access This article is licensed under a Creative Commons Attribution 4.0 International License, which permits use, sharing, adaptation, distribution and reproduction in any medium or format, as long as you give appropriate credit to the original author(s) and the source, provide a link to the Creative Commons licence, and indicate if changes were made. The images or other third party material in this article are included in the article's Creative Commons licence, unless indicated otherwise in a credit line to the material. If material is not included in the article's Creative Commons licence and your intended use is not permitted by statutory regulation or exceeds the permitted use, you will need to obtain permission directly from the copyright holder. To view a copy of this licence, visit <http://creativecommons.org/licenses/by/4.0/>.

© The Author(s) 2022